REPORT DOCUMENTATION PAGE

Form Approved
OMB No. 0704-0188

1. REPORT DATE *(DD-MM-YYYY)*	2. REPORT TYPE	3. DATES COVERED *(From - To)*
3-05-2011	Journal Article	

4. TITLE AND SUBTITLE

Synthesis, Cure Kinetics, and Physical Properties of a New Tricyanate Ester with Enhanced Molecular Flexibility

5a. CONTRACT NUMBER

5b. GRANT NUMBER

5c. PROGRAM ELEMENT NUMBER

6. AUTHOR(S)
Andrew J. Guenthner, Matthew C. Davis, Kevin R. Lamison, Gregory R. Yandek, Lee R. Cambrea, Thomas J. Groshens, Lawrence C. Baldwin, and Joseph M. Mabry

5d. PROJECT NUMBER

5f. WORK UNIT NUMBER
23030521

7. PERFORMING ORGANIZATION NAME(S) AND ADDRESS(ES)

Air Force Research Laboratory (AFMC)
AFRL/RZSM
9 Antares Road
Edwards AFB CA 93524-7401

8. PERFORMING ORGANIZATION REPORT NUMBER

AFRL-RZ-ED-JA-2011-149

9. SPONSORING / MONITORING AGENCY NAME(S) AND ADDRESS(ES)

Air Force Research Laboratory (AFMC)
AFRL/RZS
5 Pollux Drive
Edwards AFB CA 93524-7048

10. SPONSOR/MONITOR'S ACRONYM(S)

11. SPONSOR/MONITOR'S NUMBER(S)
AFRL-RZ-ED-JA-2011-149

12. DISTRIBUTION / AVAILABILITY STATEMENT

Approved for public release; distribution unlimited (PA #11096).

13. SUPPLEMENTARY NOTES
For publication in Polymer Journal

14. ABSTRACT

1,2,3-Tris(4-cyanatophenyl)propane, a new tricyanate ester monomer analogous to cyanated novolac or "phenolic triazine (PT) resin" that features more flexible chemical linkages at the central branch point, was synthesized in nine steps with an overall yield of 26%. The highly purified monomer exhibited an activation energy of 110 kJ/mol for auto-catalytic cure at temperatures of 210 °C to 290 °C, modestly lower than the comparably measured activation energy of a commercial cyanated novolac. The overall extent of cure achievable at these temperatures was also higher for the new monomer. Many physical properties of the cured monomer, including density, thermochemical stability, moisture uptake, and the impact of hydrolytic degradation on glass transition temperature were similar to those of commercial tricyanates, with a dry glass transition temperature at full conversion of at least 340 °C.

15. SUBJECT TERMS

16. SECURITY CLASSIFICATION OF:			17. LIMITATION OF ABSTRACT	18. NUMBER OF PAGES	19a. NAME OF RESPONSIBLE PERSON
					Dr. Joseph M. Mabry
a. REPORT	b. ABSTRACT	c. THIS PAGE	SAR	49	19b. TELEPHONE NUMBER *(include area code)*
Unclassified	**Unclassified**	**Unclassified**			N/A

Synthesis, Cure Kinetics, and Physical Properties of a New Tricyanate Ester with Enhanced Molecular Flexibility

Andrew J. Guenthner*[1], Matthew C. Davis[2], Kevin R. Lamison[3], Gregory R. Yandek[1], Lee R. Cambrea[2], Thomas J. Groshens[2], Lawrence C. Baldwin[2], and Joseph M. Mabry[1]

[1]Air Force Research Laboratory, Edwards AFB, CA 93524
[2]Naval Air Warfare Center, Weapons Division, China Lake, CA 93555
[3]ERC Corporation, Edwards AFB, CA 93524

Abstract

1,2,3-Tris(4-cyanatophenyl)propane, a new tricyanate ester monomer analogous to cyanated novolac or "phenolic triazine (PT) resin" that features more flexible chemical linkages at the central branch point, was synthesized in nine steps with an overall yield of 26%. The highly purified monomer exhibited an activation energy of 110 kJ/mol for auto-catalytic cure at temperatures of 210 °C to 290 °C, modestly lower than the comparably measured activation energy of a commercial cyanated novolac. The overall extent of cure achievable at these temperatures was also higher for the new monomer. Many physical properties of the cured monomer, including density, thermochemical stability, moisture uptake, and the impact of hydrolytic degradation on glass transition temperature were similar to those of commercial tricyanates, with a dry glass transition temperature at full conversion of at least 340 °C.

Keywords: cyanate ester; cure kinetics; activation energy

*correspondence to: andrew.guenthner@edwards.af.mil; 661-275-8020

1. Introduction

In recent years, the aromatic tricyanate ester[1-3] has emerged as an important class of high-performance thermosetting polymer, combining high glass transition temperatures and short-term thermal stability well in excess of 300 °C with low-cost options for composite processing such as filament winding and resin transfer molding.[4-6] As a result, tricyanate esters have been used in a growing array of applications in the aerospace industry,[7, 8] where their high stiffness, low volatility, reduced toxicity, minimal shrinkage during cure, and excellent resistance to fire and water make them extremely well-suited to the fabrication of parts with thick cross-sections. Despite their many practical advantages, however, they have received much less attention recently than bisphenol type dicyanate esters [9] in terms of basic research and the development of structure-property relationships.

The development of structure-property relationships for tricyanate esters involves significant challenges not encountered in studying most thermosetting resins. When fully cured, tricyanate esters such as the phenyl triazine (PT, or "novolac type") resins, exhibit physical cross-link densities approximately double those of the more common bisphenol type resins, owing to the central branch point (herein referred to as the "core") in the chemical structure of the monomer, which acts like a cross-link upon incorporation into the network. The high cross-link density pushes the glass transition temperature of fully trimerized systems near to, and in some cases, beyond, the limit of even short-term thermal stability of the molecules. The rigidity of the network, however, makes full trimerization very difficult to achieve in practice. Not surprisingly, then, the reported glass transition temperatures of "cured" polycyanate esters varies widely. In the case of cyanated novolac with the approximate structure shown in Figure 1, the reported dry glass transition temperature of cured resin varies from 305 °C[10] to over 400 °C[11]. In addition, the high cross-link density leads to a high level of brittleness[12], which hinders fabrication and evaluation of test specimens for mechanical property assessments. These

challenges are not only an issue for research investigations, but also represent obstacles to the widespread use of these materials in large-scale fabrication.

One promising approach to overcoming the aforementioned challenges is to synthesize new tricyanate esters with a broader range of chemical structures and, hence, physical properties. By comparing these new materials with already existing forms, structure-property relationships can be more easily discerned. At the same time, new materials that exhibit better cure and toughness characteristics can be used either in place of or as additives for existing commercial products, making tricyanate esters a more attractive choice for high-performance applications. Recently, for instance, Yameen *et al* [13] synthesized a new tricyanate ester oligomer that combined excellent flow and processing characteristics with a glass transition temperature of 280 °C, equivalent to the best-performing bisphenol type cyanate esters. Similarly, Cambrea *et al*.[14] recently synthesized a tricyanate ester monomer that flowed at room temperature and produced a dry glass transition temperature of 305 °C. In both these cases, a rigid phenyl ring was retained at the monomer core, while a lower cross-link density compared to products such as Primaset® PT-30 led to somewhat lower glass transition temperatures.

In the present work, an alternative synthesis approach to improving the performance of tricyanate esters is explored. A new tricyanate ester, designed to have the same cross-link density as Primaset® PT-30, yet with a more flexible core based on a 1,2,3-trisubstituted propane, was synthesized. The flexible core lowered the activation energy of cure, and enabled nearly complete conversion to be achieved more readily. As a result, a glass transition temperature as high as the short-term thermal stability limit for tricyanate esters was maintained. These favorable characteristics show that altering the rigidity of the core cross-link in tri-functional thermosetting macromolecules is a highly useful, though mostly unexplored, means of improving the properties of high-performance polymers.

2. Experimental

2.1. Materials

The 4-methoxyphenylacetic acid, *p*-anisaldehyde, acetic anhydride (Ac_2O), thionyl chloride ($SOCl_2$), anisole, sodium borohydride ($NaBH_4$), 5 % Pd/C catalyst, pyridine hydrochloride, cyanogen bromide (BrCN), triethylamine (TEA) as well as solvents were purchased from Sigma-Aldrich (Milwaukee) and used as received.

*2.2. Synthesis of monomer **9***

*2.2.1. (Z) 2,3-Bis(4-methoxyphenyl)acrylic acid (**1**)*

A 1 L round-bottomed flask equipped with magnetic stirring bar and reflux condenser charged with a mixture of 4-methoxyphenylacetic acid (49.8 g, 0.3 mol), *p*-anisaldehyde (40.8 g, 0.3 mol, 1 equiv), TEA (30 mL, 21.78 g, 0.07 mol) and Ac_2O (60 mL, 64.8 g, 0.21 mol) was refluxed for 4 h. The mixture was cooled to rt and H_2O (300 mL) was carefully added. The resulting pale yellow precipitate was filtered on a coarse porosity glass frit. The crude product was dissolved in a solution of KOH (16.8 g, 0.3 mol) in H_2O (1 L). The supernatant was decanted away from an insoluble residue and then vigorously stirred while neutralized with HOAc. Copious white solids precipitated. The precipitate was collected on a coarse porosity glass frit and air-dried to constant weight. The solid was recrystallized from EtOH to give the title compound as colorless needles. Yield: 44 g (52 %). Mp: 213-216 °C (lit.[15] 216-217 °C). ^{1}H NMR (DMSO-d_6) δ(ppm): 12.31 (1H, CO_2H), 7.68 (s, 1H), 7.09 (d, J = 8.6 Hz, 2H), 7.04 (d, J = 8.9 Hz, 2H), 6.95 (d, J = 8.7 Hz, 2H), 6.78 (d, J = 8.7 Hz, 2H), 3.79 (s, 3H), 3.71 (s, 3H); ^{13}C NMR (DMSO-d_6) δ(ppm): 168.75, 159.78, 158.54, 138.51, 131.84, 130.69, 130.38, 128.59, 127.01, 113.99, 113.80, 55.13, 55.01. Anal. calcd for $C_{17}H_{16}O_4$: C, 71.82; H, 5.67. Found: C, 71.75; H, 5.63. Trituration of the insoluble residue with acetone gave 2 g of a white solid. The solid was recrystallized from HOAc to give colorless flakes found

to be *trans* 4,4'-dimethoxystilbene. Mp: 214-216 °C (lit.[16] 211-212 °C). Anal. calcd for $C_{16}H_{16}O_2$: C, 79.97; H, 6.71. Found: C, 78.60; H, 6.55.

*2.2.2. racemic 2,3-Bis(4-methoxyphenyl)propionic acid (**2**)*

A mixture of **1** (44 g, 0.15 mol), 5% Pd/C (500 mg) and DMF (500 mL) was hydrogenated at rt and atmospheric pressure for 24 h. The mixture was filtered through diatomaceous earth to remove the catalyst and the filtrate was poured into H_2O (1 L). The mixture was extracted three times with EtOAc (3X 200 mL). The extracts were collected and washed with H_2O (300 mL) followed by brine (300 mL). The organic layer was separated and dried over anhydrous $MgSO_4$. Rotary evaporation of the solvent left an off-white solid. Recrystallization of the crude product from heptane/EtOAc gave the title compound as colorless needles. Yield: 40.3 g (90 %). Mp: 125-127 °C (lit.[17] 125-127 °C). ^{1}H NMR ($CDCl_3$) δ(ppm): 11.47 (bs, CO_2H), 7.19 (d, J = 8.5 Hz, 2H), 6.99 (d, J = 8.8 Hz, 2H), 6.82 (d, J = 9.1 Hz, 2H), 6.73 (d, J = 8.8 Hz, 2H), 3.78-3.69 (m, 7H), 3.29 (dd, J = 13.8 and 8.1 Hz, 1H), 2.93 (dd, J = 14.1 and 7.2 Hz, 1H); ^{13}C NMR ($CDCl_3$) δ(ppm): 180.04, 159.19, 158.33, 131.03, 130.26, 130.07, 129.34, 114.26, 113.97, 55.39, 55.33, 53.06, 38.65. Anal. calcd for $C_{17}H_{18}O_4$: C, 71.31; H, 6.34. Found: C, 71.39; H, 6.37.

*2.2.3. racemic 2,3-Bis(4-methoxyphenyl)propionyl chloride (**3**)*

A 1 L round-bottomed flask equipped with magnetic stirring bar was charged with **2** (40.3 g, 0.14 mol) and $SOCl_2$ (100 mL). A reflux condenser with N_2 bubbler piped to an aqueous NaOH gas scrubbing bottle was equipped and the mixture was gently refluxed. After 3 h, the excess $SOCl_2$ was evaporated and the crude oil was dissolve in hexanes (300 mL). After stirring briefly, the product precipitated as an off-white powder. The solid was collected by filtration on a medium porosity glass frit. Recrystallization from heptane gave the title compound as colorless needles. Yield: 33.1 g (77 %). Mp: 62-65 °C (lit.[18] 64-66 °C). ^{1}H NMR ($CDCl_3$) δ(ppm): 7.16 (d, J = 8.9 Hz, 2H), 6.98 (d, J = 8.6 Hz, 2H), 6.87 (d, J = 8.6 Hz, 2H), 6.76 (d, J = 8.6 Hz, 2H), 4.16 (t, J = 7.6 Hz, 1H), 3.77 (s, 3H), 3.74 (s, 3H), 3.39 (dd, J = 14.2 and 7.6 Hz, 1H),

2.99 (dd, *J* = 14.2 and 7.4 Hz, 1H); ^{13}C NMR ($CDCl_3$) δ(ppm): 174.75, 159.77, 158.62, 130.19, 129.79, 129.76, 127.58, 114.64, 114.09, 64.94, 55.42, 55.34, 38.86. Anal. calcd for $C_{17}H_{17}ClO_3$: C, 67.00; H, 5.62. Found: C, 67.12; H, 5.58.

*2.2.4. racemic 1,2,3-Tris(4-methoxyphenyl)propanone (**4**)*

A 500 mL round-bottomed flask equipped with magnetic stirring bar was charged with **3** (30 g, 98 mmol) and anisole (21.1 g, 196 mmol, 2 equiv) and the mixture was gently heated for complete dissolution. While vigorously stirred, $AlCl_3$ (12.9 g, 98 mmol, 1 equiv) was added portionwise. Copious HCl gas was generated during this time and the mixture became deep red in color. After all the catalyst had been added, the mixture was heated to 70 °C for 30 min. After this time, the mixture was cooled to rt and dissolved in CH_2Cl_2 (300 mL). The reaction solution was slowly quenched by adding in a gentle stream to vigorously stirred H_2O (300 mL). The organic phase was separated and washed with H_2O (300 mL) followed by saturated aqueous $NaHCO_3$ (300 mL) and finally brine (300 mL). After drying the organic phase over anhydrous $MgSO_4$, the solvent and excess anisole were evaporated leaving a crude white solid. Recrystallization from EtOH gave the title compound as a white microcrystalline powder. Yield: 32.3 g (87 %). Mp: 116-119 °C (lit.[19, 20] 122-124 °C). ^{1}H NMR ($CDCl_3$) δ(ppm): 7.89 (d, *J* = 9.0 Hz, 2H), 7.13 (d, *J* = 8.7 Hz, 2H), 6.98 (d, *J* = 8.6 Hz, 2H), 6.82 (d, *J* = 8.8 Hz, 2H), 6.78 (d, *J* = 8.7 Hz, 2H), 6.73 (d, *J* = 8.5 Hz, 2H), 4.66 (t, *J* = 7.2 Hz, 1H), 3.79 (s, 3H), 3.74 (s, 3H), 3.73 (s, 3H), 3.44 (dd, *J* = 13.7 and 7.3 Hz, 1H), 2.96 (dd, *J* = 13.9 and 7.2 Hz, 1H); ^{13}C NMR ($CDCl_3$) δ(ppm): 198.37, 163.43, 158.79, 158.11, 132.36, 131.86, 131.16, 130.29, 130.05, 129.49, 114.45, 113.86, 113.83, 55.59, 55.39, 55.06, 39.50. Anal. calcd for $C_{24}H_{24}O_4$: C, 76.57; H, 6.43. Found: C, 76.55; H, 6.43.

*2.2.5. racemic 1,2,3-Tris(4-methoxyphenyl)propanol (**5**)*

A 2 L round-bottomed flask equipped with magnetic stirring bar and reflux condenser was charged with **4** (32.3 g, 85 mmol) and anhydrous EtOH (500 mL). In several portions, $NaBH_4$ (4.6 g, 121 mmol, 1.4

equiv) was added and the mixture was heated to reflux. After 3 h, the reaction was complete by TLC. The mixture was carefully diluted with H_2O (500 mL) and stirred for 1 h. The mixture was extracted Et_2O (3X 300 mL). The organic phases were collected and washed with H_2O (300 mL) followed by 300 mL brine. After drying over anhydrous $MgSO_4$, the organic layer was rotary evaporated leaving the title compound as a viscous, colorless oil. Yield: 30.68 g (95 %). ^{1}H NMR ($CDCl_3$) δ(ppm):.23-6.99 m, 4H), 6.92-6.60 (m, 8H), 4.81 (d, *J* = 6.3 Hz, 25% 1H), 4.74 (d, *J* = 7.5 Hz, 75% 1H), 3.87-3.62 (m, 9H), 3.26-2.57 (m, 3H), 1.83 (bs, OH); ^{13}C NMR ($CDCl_3$) δ(ppm): 159.38, 158.66, 157.87, 135.21, 132.52, 132.49, 130.24, 130.17, 130.05, 128.24, 127.98, 114.00, 113.92, 113.68, 113.59, 113.54, 55.88, 55.47, 55.37, 55.32, 55.28, 38.12. Anal. calcd for $C_{24}H_{26}O_4$: C, 76.17; H, 6.92. Found: C, 76.37; H, 7.04.

*2.2.6. (E/Z) 1,2,3-Tris(4-methoxyphenyl)propene (**6**)*

A 1 L round-bottomed flask equipped with magnetic stirring bar and reflux condenser with Dean-Stark attachment was charged with **5** (30.68 g, 81 mmol), toluene (500 mL) and *p*-toluenesulfonic acid dihydrate (380 mg). The mixture was brought to reflux and after 1 h the dehydration was complete. After cooling to rt, the mixture was washed with saturated aqueous $NaHCO_3$ (300 mL) followed by brine (300 mL). After drying over anhydrous $MgSO_4$, the solvent was rotary evaporated leaving the title compound as a viscous, colorless oil. Yield: 27.7 g (95 %). ^{1}H NMR ($CDCl_3$) δ(ppm): 7.39-6.23 (m, 13H), 3.96 (s, 60% 2H), 3.74-3.64 (m, 9H), 3.59 (s, 40% 2H); Anal. calcd for $C_{24}H_{24}O_3$: C, 79.97; H, 6.71. Found: C, 80.23; H, 6.76.

*2.2.7. 1,2,3-Tris(4-methoxyphenyl)propane (**7**)*

A mixture of **6** (27.7 g, 77 mmol), 5 % Pd/C (1 g) and EtOH (500 mL) was hydrogenated (2 psi) for 18 h. The mixture was filtered through diatomaceous earth and rotary evaporated leaving the crude product. Reduced pressure distillation (0.1 torr) gave the title compound as a viscous, colorless oil. Yield: 26.5 g (95 %). ^{1}H NMR ($CDCl_3$) δ(ppm): 6.89-6.78 (m, 6H), 6.69-6.61 (m, 6H), 3.68 (s, 3H), 3.67 (s, 6H), 2.98-2.64

(m, 5H); ^{13}C NMR ($CDCl_3$) δ(ppm): 157.97, 157.87, 136.73, 132.96, 130.24, 129.00, 113.65 (2 overlapping signals), 55.37, 55.34, 49.57, 41.88. Anal. calcd for $C_{24}H_{26}O_3$: C, 79.53; H, 7.23. Found: C, 79.69; H, 7.26.

*2.2.8. 1,2,3-Tris(4-hydroxyphenyl)propane (**8**)*

A 500 mL round-bottomed flask equipped with magnetic stirring bar and reflux condenser was charged with **7** (26.5 g, 73 mmol) and pyridine hydrochloride (102 g, 12 equiv). The mixture was refluxed for 3 h by heating mantle after which time TLC showed the reaction was complete. The mixture was cooled and carefully quenched with H_2O (500 mL). The mixture was extracted with Et_2O (3X 200 mL). The extracts were collected and washed with 5 % HCl (300 mL) followed by H_2O (500 mL) and finally brine (500 mL). After drying over anhydrous $MgSO_4$, the solvent was evaporated leaving a thick colorless residue. Recrystallization from toluene gave the title compound as a white microcrystalline powder. Yield: 22 g (94 %). Mp: 161-163 °C (lit.[19, 20] 164 °C). ^{1}H NMR ($CDCl_3$/DMSO-d_6) δ(ppm): 8.19 (bs, 3 OH), 6.86-6.75 (m, 6H), 6.65 (d, J = 8.9 Hz, 2H), 6.64 (d, J = 8.3 Hz, 4H), 3.02 (m, 5H); ^{13}C NMR ($CDCl_3$/DMSO-d_6) δ(ppm): 154.74, 154.68, 135.03, 131.22, 129.64, 128.44, 114.77, 114.73, 48.95, 41.41, 20.69. Anal. calcd for $C_{21}H_{20}O_3$: C, 78.73; H, 6.29. Found: C, 78.59; H, 6.34.

*2.2.9. 1,2,3-Tris(4-cyanatophenyl)propane (**9**)*

A 500 mL round-bottomed flask equipped with magnetic stirring bar and 100 mL addition funnel was charged with **8** (26 g, 81 mmol), BrCN (30.1 g, 284 mmol, 3.5 equiv) and anhydrous acetone (500 mL). The mixture was cooled in a -20 °C bath and TEA (24.6 g, 33.8 mL, 244 mmol, 3 equiv) was added dropwise over 30 min. Copious solids (TEA·HBr) precipitated during the addition. The mixture was stirred in the cooling bath for 2 h and then allowed to warm to rt. The reaction was quenched by slowly adding H_2O (400 mL) whereby the by-product salt dissolved and the product precipitated concominantly. The white solid was collected on a coarse porosity glass frit and air-dried under suction for several hours. The crude product was recrystallized from *i*-PrOH to give the title compound as

colorless needles. Yield: 25.12 g (78 %). Mp: 102-104 °C. ^{1}H NMR ($CDCl_3$) δ(ppm): 7.19-7.11 (m, 6H), 7.09-6.99 (m, 6H), 3.18-3.00 (m, 3H), 2.97-2.85 (m, 2H); ^{13}C NMR ($CDCl_3$) δ(ppm): 151.55, 151.49, 141.64, 138.41, 130.96, 129.81, 115.51, 115.38, 108.90, 108.81, 49.50, 41.83. Anal. calcd for $C_{24}H_{17}N_3O_3$: C, 72.90; H, 4.33; N, 10.63. Found: C, 72.67; H, 4.25; N, 10.59.

2.3. Characterization

2.3.1 Monomer characteristics

Melting points were collected on a Mel-Temp II from Laboratory Devices (Holliston, MA) and are not corrected. Infrared analysis of monomer **9** and all cured and uncured samples, were analyzed by Attenuated Total Reflection Fourier Transform Infrared (ATR-FTIR) spectroscopy using a single bounce diamond ATR crystal. The instrument used was a Nexus 870 FTIR spectrometer with a liquid N_2 cooled mercury cadmium telluride (MCTA) detector. Each spectrum is an average of 28 scans at 4 cm^{-1} resolution. ^{1}H NMR and ^{13}C NMR were collected on a Bruker Avance II 300 MHz spectrometer operated at 300 and 75 MHz respectively. Nuclear magnetic resonance data (free-induction decays) were processed using NUTS software from Acorn NMR (Livermore, CA). All spectra are referenced to solvent or tetramethylsilane. Elemental analyses were performed by Atlantic Microlab, Inc. (Norcross, GA).

CCDC 802927 (**9**) contains the supplementary crystallographic data for this paper. These data can be obtained free of charge from The Cambridge Crystallographic Data Centre via www.ccdc.cam.ac.uk/data_request/cif, by e-mailing data_request@ccdc.cam.ac.uk, or by contacting CCDC 12 Union Road, Cambridge CB2 1EZ, UK; fax: +44 1223 336033.

2.3.2 Cure kinetics

Studies of cure kinetics were performed via differential scanning calorimetry (DSC) using ~5 mg samples of uncatalyzed monomers and a TA Instruments Q200 Differential Scanning Calorimeter under 50 mL / min. of flowing nitrogen. The samples were first heated to 120 °C at 5 °C / min. in order to produce molten material, then held at 120 °C for 5 minutes to equilibrate and establish a baseline. The samples were then heated as rapidly as possible (maximum rate of around 100 °C / min.) to the intended cure temperature, and held at that temperature for 30 minutes. Following the hold at the cure temperature, the samples were cooled as rapidly as possible (ca. 100 °C / min.) to 120 °C, and then re-heated to 350 °C at 10 °C / min. to determine the residual enthalpy of polymerization. Cure temperatures of 210 °C to 290 °C in increments of 20 °C were used.

To analyze the cure data, both the rate of conversion ($d\alpha/dt$) and the total conversion (α) were determined as follows:

$$\frac{d\alpha(t)}{dt} = \frac{\dot{Q}(t)}{Q_T + Q_R} \;\therefore\; \alpha(t) = \frac{\int_{t_0}^{t} \dot{Q}(t')dt'}{Q_T + Q_R} \tag{1}$$

where $\dot{Q}$ represents the baseline corrected differential heat flow, Q_T is the total integrated heat flow (enthalpy of cure) observed during the isothermal cure period beginning at t_0, and Q_R is the sum of all residual heat flow associated with resin cure observed on subsequent thermal cycling to 350 °C. Since the cure of uncatalyzed cyanate esters is expected to be auto-catalytic and to follow an n-th order model with non-integer exponents (in contrast to catalyzed systems that show second-order kinetics),[21] the cure data were fitted over the range α = 0.1 to 0.5 (prior to the onset of significant diffusion-controlled cure) to the Kamal model,[22] namely:

$$\frac{d\alpha}{dt} = k_1'(1-\alpha)^n + k_2'\alpha^m(1-\alpha)^n \quad (2)$$

To fit the data, a modified form of the graphical analysis developed by Kenny[23] was used. The method took advantage of the fact that for the data collected, $k_1' << k_2'$, therefore the conversion at which the rate of cure was maximum (α_{max}) was very well approximated by the quantity m / (m+n). Since α_{max} was readily observed at multiple temperatures and was independent of temperature for a given material, its value was used to constrain the fitting process. A preliminary value of the catalytic rate constant, k_1', was first determined via extrapolation of the raw data per Kenny's method. Next, a trial value for n was chosen, and, in accordance with the following rearrangement of Eq. (2) using preliminary rate constants

$$ln\left[\frac{\frac{d\alpha}{dt}}{(1-\alpha)^n} - k_1'\right] = \ln k_2' + m\ln\alpha \quad (3)$$

the quantity of the left-hand side of Eq. (3) was plotted as a function of ln α, enabling the computation of m and k_2' via linear regression. The value of m was then iteratively adjusted via the Newton-Raphson method until the computed value of n and the chosen value of m satisfied the constraint α_{max} = m / (m + n). Due to the special features of the particular data set being analyzed, this modified method allowed values of all of the Kamal model parameters to be determined through the solution of an objective equation of the form f(dα/dt, α, α_{max}, k_1', k_2', m, n) = 0 with the straightforward ability to determine α_{max} replacing the need to judge the straightness of lines formed by plots of transformed data. For the data under consideration, iterative solution of the objective equation proved to be highly robust, and was therefore judged to be a more appropriate method than the more generally applicable graphical method described by Kenny.

To determine the activation energies, values of m and n were first determined separately for all suitable data sets describing a single material. The mean values, $\bar{m}$ and $\bar{n}$, were then utilized to

calculate refined values of the rate constants k_1 and k_2 using a linear regression of the Kamal model in the following form

$$\frac{\frac{d\alpha}{dt}}{(1-\alpha)^{\bar{n}}} = k_1 + k_2\alpha^{\bar{m}} \quad (4)$$

in which a plot of the left-hand side of Eq. (4) as a function of $\alpha^{\bar{m}}$ yields an intercept of k_1 and a slope of k_2. When, as expected, the values of m and n did not vary significantly with temperature, the values of k_1' and k_2' closely approximated the values of k_1 and k_2. The use of $\bar{m}$ and $\bar{n}$ was necessitated by the presence of significant systematic correlations among the fitted values of k_2', m, and n that could have potentially biased the calculation of activation energies. Additional details describing the collection (section S1) and analysis (section S2) of the kinetic data are provided in the Supplementary Content.

2.3.3 Cured resin sample preparation and characterization

Cured resin samples were prepared by either melting the monomer powder, or thinning the monomer liquid in the case of Primaset® PT-30, at 120 °C under a reduced pressure of 300 mm Hg for 30 minutes, followed by pouring into either a reinforced silicone casting mold (either 13 mm diameter x 3 mm discs, or 87 mm x 12 mm x 2.5 mm bars) for multi-step cure, or into a 6 mm diameter x 1 mm high aluminum pan for single-step cure. Multi-step cure involved heating in an oven under nitrogen to 150 °C for 1 hour, followed by 210 °C for 24 hours, with subsequent cooling to below 150 °C prior to de-molding. Heating ramps were 5 °C / min. Some multi-step cured samples were then post-cured as free-standing parts at temperatures of up to 290 °C. The single-step cured samples were heated in a small furnace under a nitrogen flow of 50 mL / min. with the temperature controlled to within 2 °C, at temperatures of 210 °C to 290 °C, using the maximum possible ramp rates (typically 50 – 100 °C / min.). Additional details such as the mold fabrication procedures have been published elsewhere.[24]

Thermomechanical analysis of cured samples was performed using a TA Instruments Q400 thermomechanical analyzer (TMA) in dynamic (oscillatory compression) TMA mode. The oscillatory compression mode provides qualitative information on the storage and loss components of the sample stiffness, in addition to sample displacement as a function of temperature. Due to the very high glass transition temperatures of the samples studied and their tendency to post-cure during heating to high temperatures, very rapid heating and cooling rates of 50 °C / min were used. A standard thermal cycling procedure, using limits of 0 °C and 200 °C, was used to determine and correct for the thermal lag caused by these rapid heating rates. The procedure was employed prior to heating to 400 °C for dry samples, and after heating to 350 °C for wet samples. The mean compressive load on the samples was 0.1 N, with an oscillatory force applied at an amplitude of 0.1 N and a frequency of 0.05 Hz. Complete details, examples, and the rationale for the cycling procedures have been explained at length elsewhere.[24] Thermogravimetric analysis (TGA) was carried out using a TA Instrument Q5000 under 60 mL / min. of either nitrogen or air. For TGA analysis, ~ 2 mg of uncured powder was heated at 10 °C / min. to 600 °C. The density of cured samples was determined via neutral buoyancy of 13 mm x 3 mm discs in $CaCl_2$ / deionized water mixtures, as described elsewhere.[25] Some multi-step cured and post-cured samples were placed in 250 mL of deionized water at 85 °C for 96 hours as a means of testing the effects of exposure to hot water.

3. Results and discussion

*3.1. Synthesis of tricyanate monomer **9***

The synthesis of tricyanate monomer **9** is shown in Scheme 1. Perkin condensation of 4-methoxyphenylacetic acid on anisaldehyde gave the 2,3-diarylacrylic acid **1** in modest yield.[26-29] Catalytic hydrogenation of **1** in dimethylformamide solvent gave the propionic acid **2** in excellent yield. Following acid chloride generation, standard Friedel-Crafts reaction of **3** with anisole gave the racemic

ketone **4** previously reported by Kiprianov and Kutsenko in good yield.[19, 20] Reduction of **4** with sodium borohydride gave a diastereomeric mixture of alcohol **5**. Acid-catalyzed dehydration of **5** gave a cis/trans mixture of 1,2,3-triarylpropene **6** which was then hydrogenated to give **7**. The penultimate step was demethylation of **7** with molten pyridine hydrochloride which gave the solid triphenol **8** in excellent yield. Finally, reaction of **8** with cyanogen bromide in the presence of triethylamine gave the solid tricyanate **9** in good yield. The ^{1}H and ^{13}C NMR of **9** is shown in Figure 2. The monomer **9** could be readily recrystallized from alcoholic solvents and a crystal structure was obtained, Figure 3.

*3.2. Cure kinetics of monomer **9***

When discussing the cure kinetics of cyanate esters, it is especially important to take into consideration the effects of catalytic impurities. Truly pure cyanate ester resins may not cure at all below their chemical decomposition temperatures,[30] and the overall rates of cure are known to depend very strongly on the level of phenolic and other impurities.[21, 31] The NMR, elemental, and X-ray analyses of monomer **9** were all indicative of impurities on the order of 1% at most, and although no specific impurities were identifiable, based on previous syntheses of cyanate esters,[4, 32] partially cyanated phenolic compounds would be expected to constitute the majority of any impurities present. Although a detailed purity analysis could provide additional insights into expected cure kinetics, it is much simpler to focus on aspects of cure that are typically affected only modestly by impurities. For cyanate esters, the total enthalpy of cyclotrimerization per equivalent appears to be constant (within experimental error)[4] for systems not intentionally catalyzed, and to show a very modest decrease in systems catalyzed by transition metals.[24] The activation energy at elevated temperatures also appears to be insensitive to impurities, and to decrease only moderately when transition metal catalysts are present.[33, 34] Thus, the enthalpy and activation energy of cure were the focus of our analysis.

A sense of the overall cure kinetics of monomer **9** in comparison to Primaset® PT-30, a commercially available novolac-type cyanate ester resin, is provided by the non-isothermal DSC thermograms shown in Figure 4. In both cases, the cure exotherm peaked at over 300 °C, typical for a high purity cyanate ester monomer.[35, 36] The enthalpies of cure were also similar, at 750 J/g (99 kJ/eq.) for monomer **9** and 660 J/g for PT-30. The enthalpy of cure for monomer **9** on a cyanate ester equivalent basis was well within the expected range[4, 21] while that of PT-30 agreed well with previously reported values.[37] Based on multiple DSC samples heated past the melting point, monomer **9** exhibited a melting endotherm with a peak temperature of 107.4 ± 0.2 °C and an enthalpy of melting of 83 ± 1 J / g. No glass transition temperatures below 350 °C (at which point thermal degradation begins to interfere with DSC analysis) were observed in the second heating scans of either sample.

More detailed data on the kinetics of cure was provided by the isothermal DSC data summarized in Figures 5a (for monomer **9**) and 5b (for Primaset® PT-30). A visual comparison of the two Figures clearly reveals a more modest temperature dependence of the kinetics of cure for monomer **9**, indicative of a lower activation energy. Though somewhat complex, the mathematical analysis of the kinetic data is merely an elaboration on the preceding observation for the sake of quantification, with care being taken not to bias the results through the choices inherent in the analysis method. A detailed discussion may be found in section S2 of the Supplementary Content.

The results of the kinetic analysis are summarized by the Arrhenius plot of Figure 6, which is based on the auto-catalytic rate constant (k_2) with temperature-independent reaction order exponents. The activation energy for monomer **9** was modestly lower, at 110 ± 2 kJ/mol, than for PT-30 (124 ± 7 kJ/mol). The activation energies of cyanate ester cure vary widely,[21] and the choice of kinetic model can affect the values substantially, nonetheless these values appear higher than those reported for

more flexible dicyanate cyanate esters measured using similar techniques and confirmed via multiple methods.[38] Importantly, the overall rates of cure were similar for both materials through most of the temperature range, implying the absence of any significant differences in catalytic impurity levels that could affect the activation energy. At temperatures approaching 300 °C, the PT-30 did cure at a substantially faster rate, as would be expected based on the non-isothermal DSC data shown in Figure 4.

Although the PT-30 cured more rapidly than monomer **9** at elevated temperatures, FT-IR analysis of the monomers, as highlighted in Figures 7a (monomer **9**) and 7b (PT-30), reveals that for single-step cure at 290 °C, monomer **9** achieved a higher absolute extent of cure. Although these simple types of FT-IR comparisons cannot be considered strictly quantitative, the observed difference in the observed peak intensities near 2250 cm^{-1} (indicative of residual cyanate ester groups) were substantial enough to clearly show that a lower overall degree of cure was achieved in PT-30 despite more rapid kinetics. The ability of monomer **9** to achieve a greater extent of cure was most likely due to its decreased rigidity compared to PT-30, which allowed greater molecular motion even after a significant cross-link density was produced, and in turn enabled the residual cyanate ester groups to more easily rearrange themselves to accommodate cyclotrimerization. Such decreased rigidity at a molecular level should be manifest in numerous ways involving the thermomechanical and thermochemical behavior of the resins, which, given the high glass transition temperatures of the fully cured resins, are likely to be closely coupled.

3.3. Physical properties

Figure 8 shows oscillatory TMA data on both cured **9** and PT-30 samples. The TMA data shown in these Figures compares samples after cure for 24 hours at 210 °C followed by 30 minutes of post-cure at 290 °C. Such a multi-step cure was needed in order to prepare uncatalyzed cyanate ester samples of sufficient size and quality for mechanical analysis, because a single jump to 290 °C resulted in the

production of a significant quantity of volatiles (most likely due to an appreciable vapor pressure of the monomer itself at this temperature). By achieving the maximum extent of cure practically attainable at 210 °C, both the generation of volatiles as well as previously observed thermochemical degradation of the cyanate ester network during the subsequent post-cure was minimized. Note also that thermochemical degradation of the samples began to take place before the completion of the scan, thus the drop in stiffness was likely due to both physical and chemical changes in the sample.

As seen in Figure 8a, the dry glass transition temperatures for both samples are very high, at least 340 °C for cured **9** and at least 390 °C for Primaset® PT-30. Thus, the data in Figure 8 are in agreement with previously observed[11] values for the glass transition temperature of fully cured PT-30. The earlier termination of the TMA run was due to an apparent decrease in the thermochemical stability of the cured **9**. Although the notional softening point may also have been lower than that of PT-30, the TMA data reveal that the maximum use temperature under dry conditions was determined by chemical stability considerations. Thus, for well-cured, dry samples, the increased flexibility did not directly impact maximum use temperatures through a lower (notional) softening point.

Figure 8b shows TMA scans for samples exposed to 85 °C water for 96 hours (the cooling scan is shown because it is unaffected by instabilities related to the rapid drying of the sample during heating; the heating scan is provided in Section S3 of Supplementary Content and shows similar glass transition temperature amid a much noisier signal). Both cured **9** and Primaset® PT-30 exhibited glass transition temperatures around 245 °C. The weight gain on exposure for identically cured samples was about 3.5% for cured **9** compared to 5.1% for Primaset® PT-30. The improved relative performance of cured **9** under wet conditions could result from better hydrolytic stability and lower moisture uptake, however, it could also result partly from the fact the mechanical softening alone, rather than a combination of mechanical and chemical changes, determined the glass transition temperature under these conditions. These data

also indicate that for many applications, in which performance under wet conditions is a key design consideration, there will be little or no difference in maximum allowable use temperature between cured **9** and Primaset® PT-30.

Figure 9 shows the TGA curves under both nitrogen and air for cured **9** (Figure 9a) and Primaset® PT-30 (Figure 9b). In accord with the TMA results described earlier, cured **9** showed decreased thermal stability under both nitrogen and air compared to PT-30, with the onset of degradation about 30 °C lower, and about twice as much mass loss. These results make sense given the higher proportion of aliphatic groups in monomer **9**. Thus, the decreased thermochemical stability (rather than a lower softening point) was one of the primary trade-offs for the enhanced flexibility created by the choice of molecular architecture. It should be noted that the thermochemical stability of cured **9** was nonetheless quite good in comparison with many types of thermosetting polymers, including dicyanate esters, with a char yield near 50% at 600 °C in air. Additional physical properties, such as density and nominal cross-link density, are shown in Table 1.

4. Conclusions

A new tricyanate ester monomer featuring flexible chemical linkages at the central branch point [1,2,3-tris(4-cyanatophenyl)propane] has exhibited a number of useful performance improvements over a more rigid analog (Primaset® PT-30). In particular, the new monomer, which was synthesized in nine steps with an overall yield of 26%, exhibited an activation energy of 110 kJ/mol for auto-catalytic cure at temperatures of 210 °C to 290 °C, 14 kJ/mol lower than the activation energy of Primaset® PT-30 under identical conditions. The overall extent of cure achievable at temperatures of 290 °C was also higher for the new monomer. In terms of physical properties, the new monomer showed a dry glass transition temperature of at least 340 °C, likely limited by a somewhat lower thermochemical stability compared to Primaset® PT-30, while both materials exhibited a wet glass transition temperature around 245 °C.

These results indicate that many of limitations associated with rigid thermosetting monomers having a high cross-link density may be overcome with only modest trade-offs through a carefully chosen introduction of flexible elements in the molecular architecture.

Acknowledgements

Financial support through an In-house Laboratory Independent Research award from the Office of Naval Research, as well as funding from the Air Force Office of Scientific Research, is gratefully acknowledged.

Supplementary Content Available

Supplementary Content is freely available in PDF form.

References

1. Lin CH, Yang KZ, Leu TS, and Sie JW. J Polym Sci, Part A: Polym Chem 2006;44(11):3487-3502.
2. Papathomas KI. US Patent 5,292,861; 1994.
3. Jackson RJ. US Patent 4,916,210; 1990.
4. Hamerton I. Chemistry and Technology of Cyanate Ester Resins. London: Chapman & Hall, 1994.
5. Fang T and Shimp DA. Prog Polym Sci 1995;20(1):61-118.
6. Nair CPR, Mathew D, and Ninan KN. Cyanate ester resins, recent developments. New Polymerization Techniques and Synthetic Methodologies, Adv Polym Sci vol. 155, 2001. pp. 1-99.
7. McConnell VP. Resins for the Hot Zone Part II: BMIs, CEs, Benzoxazines & Phthalonitriles. High Performance Composites, 2009. pp. 43-49.
8. Wienhold PD and Persons DF. SAMPE Journal 2003;39(6):6-17.
9. Reams JT, Boyles DA. J Appl Polym Sci 2011;121(2):756-763.
10. Ganguli S, Dean D, Jordan K, Price G, and Vaia R. Polymer 2003;44(22):6901-6911.
11. Marella V. Masters Thesis. Drexel University; 2008.
12. Ganguli S, Dean D, Jordan K, Price G, and Vaia R. Polymer 2003;44(4):1315-1319.
13. Yameen B, Duran H, Best A, Jonas U, Steinhart M, and Knoll W. Macromol Chem Phys 2008;209(16):1673-1685.
14. Cambrea LR, Davis MC, Groshens TJ, Guenthner AJ, Lamison KR, and Mabry JM. J Polym Sci, Part A: Polym Chem 2010;48(20):4547-4554.
15. Ketcham R and Jambotka D. J Org Chem 1963;28(4):1034-1037.
16. Spatz SM. J Org Chem 1961;26(10):4158-4161.
17. Meyers MJ, Sun J, Carlson KE, Marriner GA, Katzenellenbogen BS, and Katzenellenbogen JA. J Med Chem 2001;44(24):4230-4251.
18. Kölling H, Lettré H. US Patent 2,691,044; 1954.
19. Kiprianov GI and Kutsenko LM. Ukranian Chemistry Journal 1957;23:505-509.
20. Kiprianov GI and Kutsenko LM. Chemical Abstracts 1958;52:6280a.
21. Hamerton I, Emsley AM, Howlin BJ, Klewpatinond P, and Takeda S. Polymer 2003;44(17):4839-4852.
22. Kamal MR and Sourour S. Polym Eng Sci 1973;13(1):59-64.
23. Kenny JM. J Appl Polym Sci 1994;51(4):761-764.
24. Guenthner AJ, Yandek GR, Mabry J M, Lamison KR, Vij V, Davis MC, and Cambrea LR. Insights into moisture uptake and processability from new cyanate ester monomer and blend studies. SAMPE International Technical Conference, vol. 55. Salt Lake City, UT: SAMPE International Business Office, 2010. pp. 42ISTC-119.
25. Lamison KR, Guenthner A J, Vij V, and Mabry JM. Packing Fraction and Relation to Glass Transition in Ternary Blends of Cyanate Ester Resins. PMSE Prepr, vol. 104, 2011.
26. Buckles RE and Bremer K. Org Synth 1953;33:70-72.
27. Oxley P and Short WF. GB Patent 559,024; 1944.
28. Green FD, Adam W, and Cantrill JE. J Am Chem Soc 1961;83(16):3461-3468.
29. Ruan B, Yang Y, Zhu Z, Lu P, and Zhu H. Acta Crystallogr Sect E Struct Rep Online 2009;65:o944.
30. Bauer M. Thesis. Academy of Sciences of the GDR; 1980.
31. Georjon O, Galy J, and Pascault JP. J Appl Polym Sci 1993;49(8):1441-1452.
32. Guenthner AJ, Yandek GR, Wright ME, Petteys BJ, Quintana R, Connor D, Gilardi RD, and Marchant D. Macromolecules 2006;39(18):6046-6053.
33. Yan HQ, Ji L, and Qi GR. J Appl Polym Sci 2004;91(6):3927-3939.
34. Recalde IB, Recalde D, García-Lopera R, and Gómez CM. Eur Polym J 2005;41(11):2635-2643.

35. Laskoski M, Dominguez DD, and Keller TM. J Polym Sci, Part A: Polym Chem 2006;44(15):4559-4565.
36. Zhao L and Hu XA. Polymer 2010;51(16):3814-3820.
37. Chen CC, Don TM, Lin TH, and Cheng LP. J Appl Polym Sci 2004;92(5):3067-3079.
38. Sheng X, Akinc M, and Kessler MR. J Therm Anal Calorim 2008;93(1):77-85.

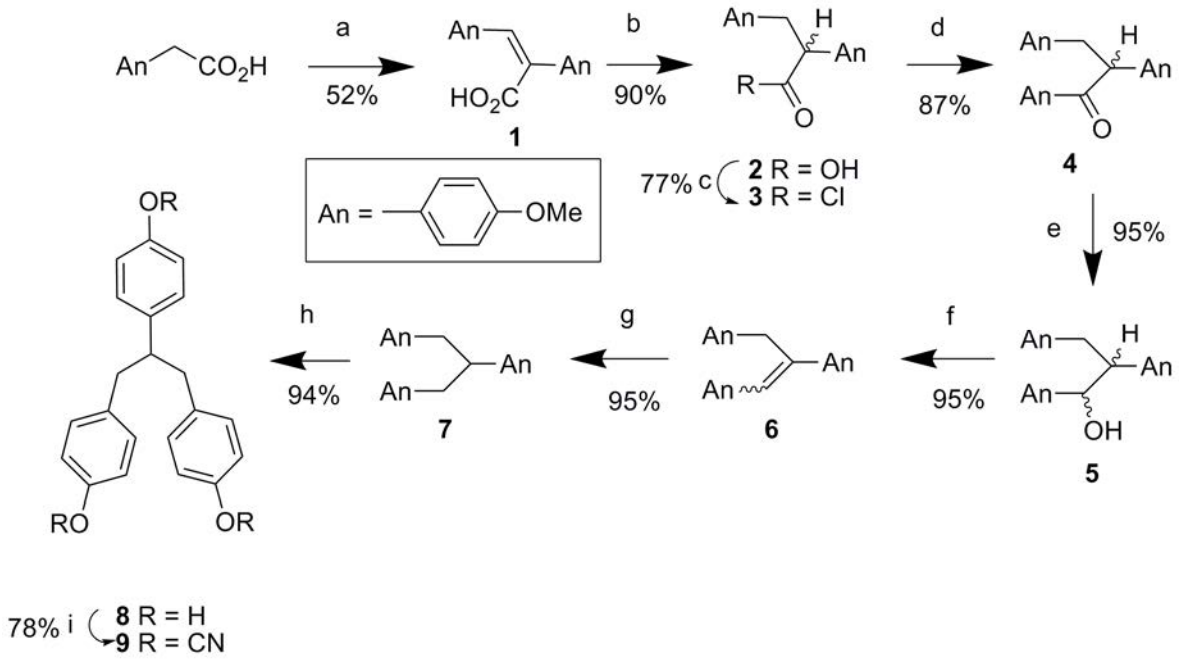

Scheme 1. Synthesis of monomer **9**: (a) 4-$MeOC_6H_4CHO$, Ac_2O, TEA, reflux; (b) H_2, 5% Pd/C, DMF; (c) $SOCl_2$, heat; (d) anisole, $AlCl_3$; (e) $NaBH_4$, EtOH; (f) *p*TsOH, PhMe, reflux; (g) H_2, 5% Pd/C, EtOH; (h) pyridine HCl, reflux; (i) BrCN, TEA, acetone, -20 °C.

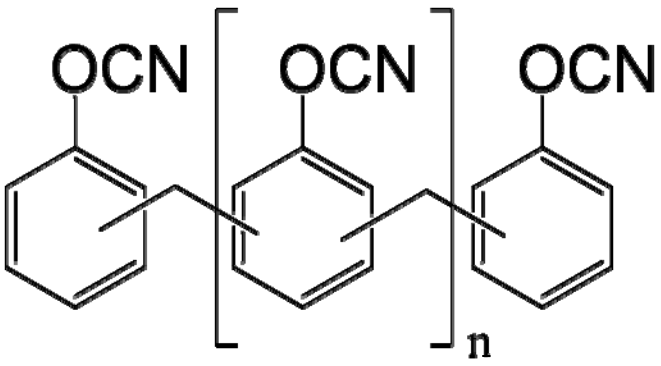

Figure 1. Approximate chemical structure (n=1-2) for Primaset® PT-30 resin.

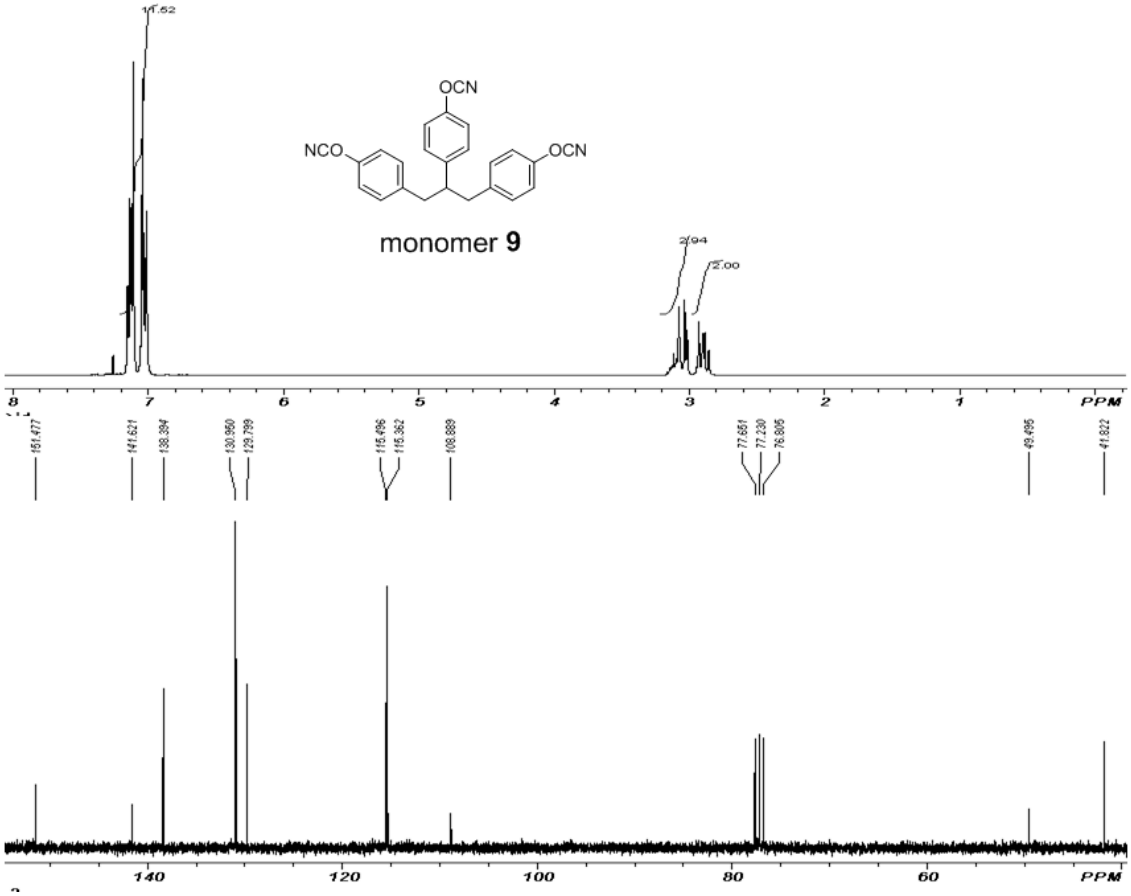

Figure 2. ^{1}H and ^{13}C NMR for monomer **9**.

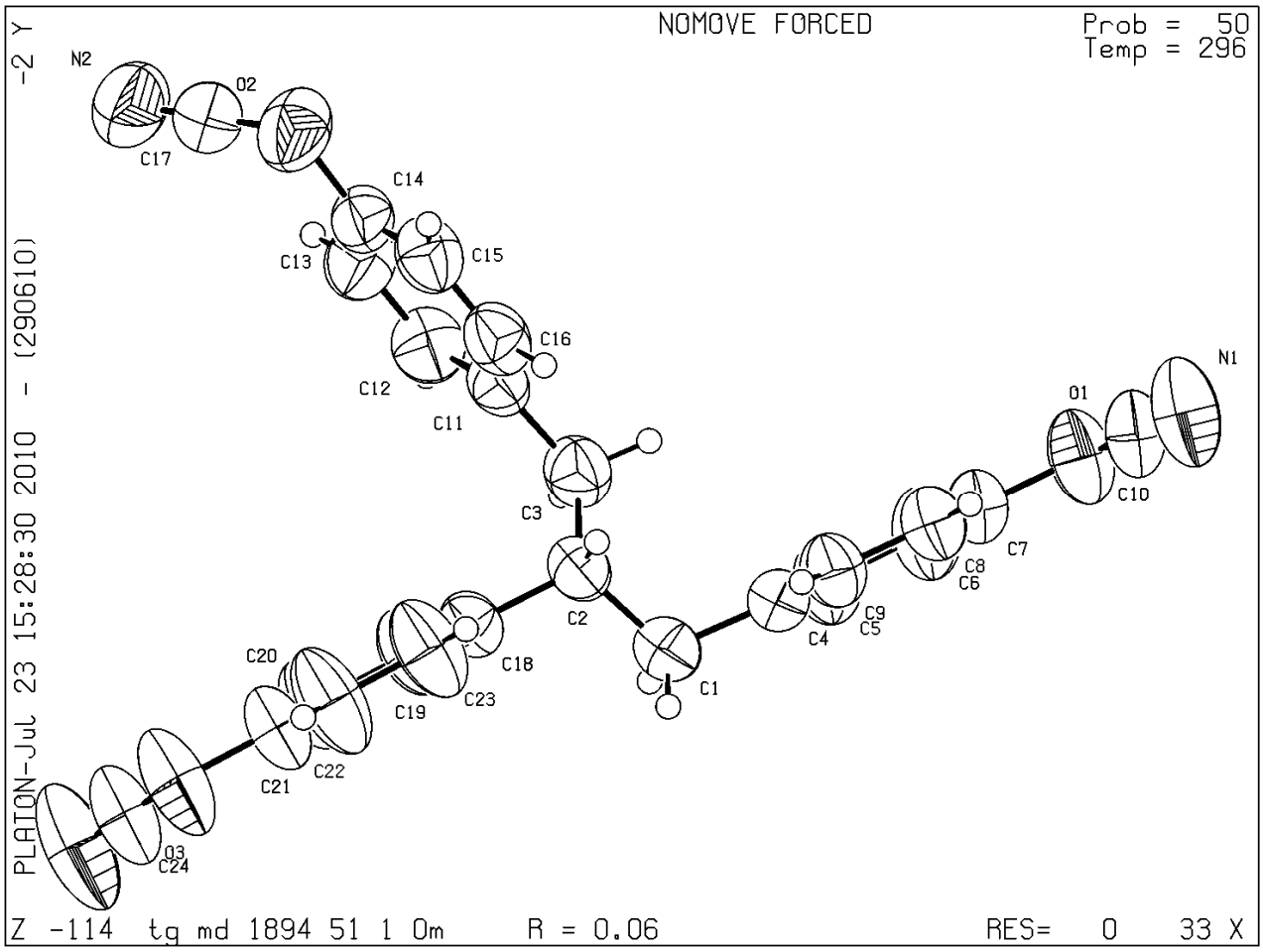

Figure 3. Crystal structure of monomer **9**.

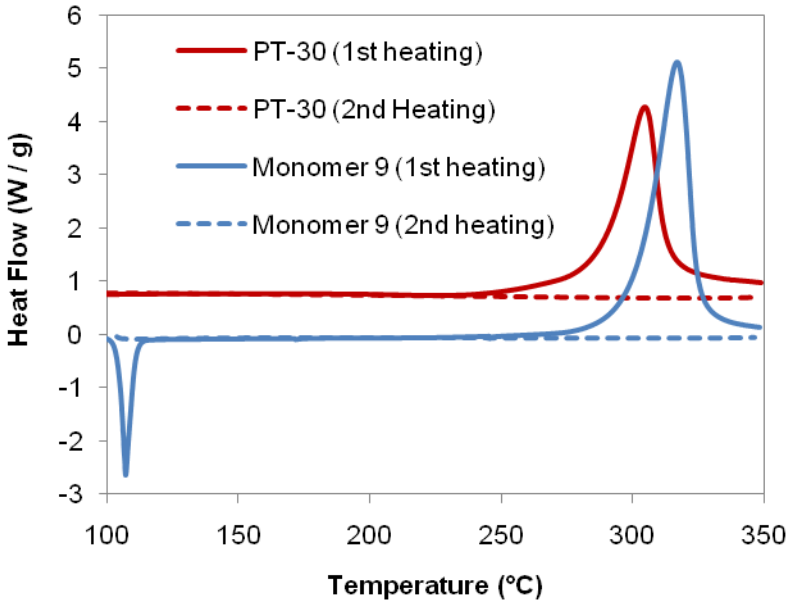

Figure 4: Non-isothermal DSC of monomer **9** and Primaset® PT-30

(a)

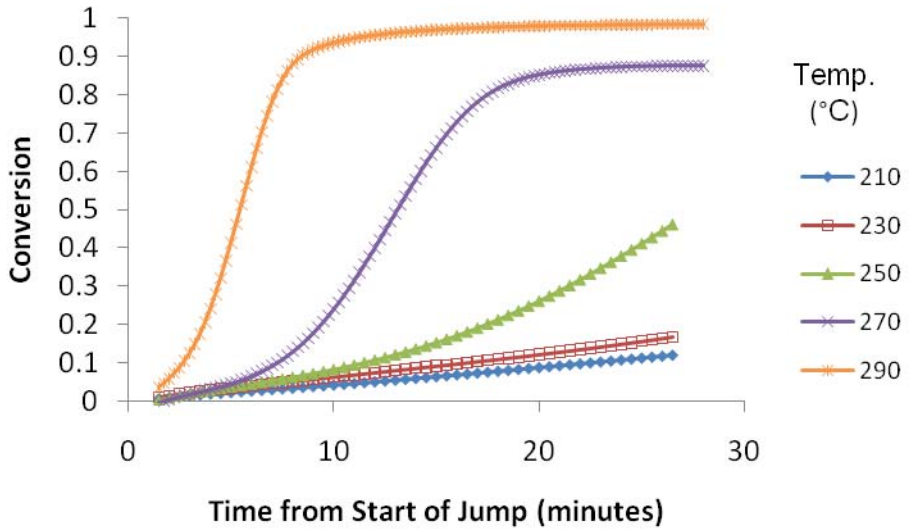

(b)

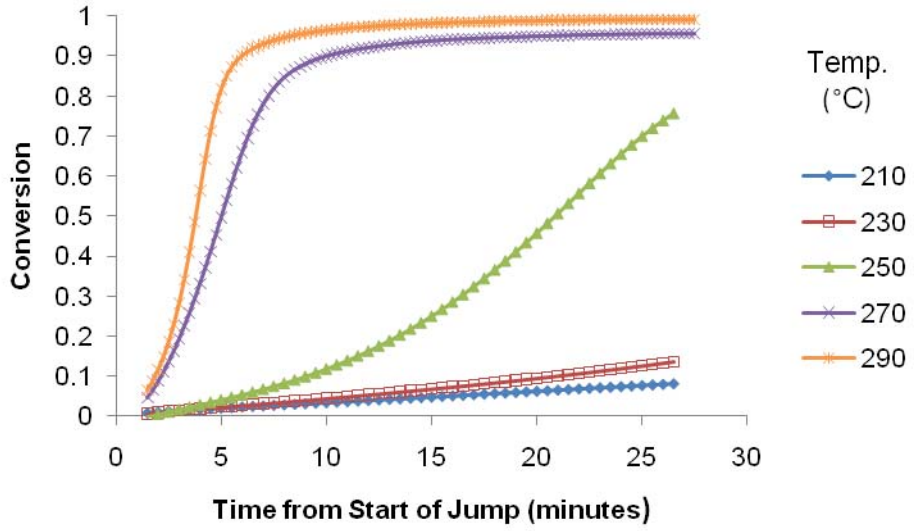

Figure 5: Isothermal conversion history of (a) monomer **9** and (b) PT-30 as a function of cure temperature

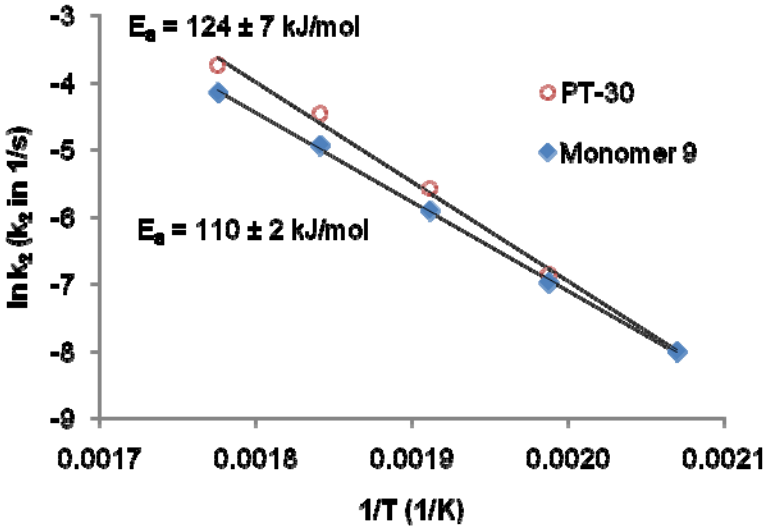

Figure 6: Autocatalytic cure activation energy of monomer **9** and PT-30

(a)

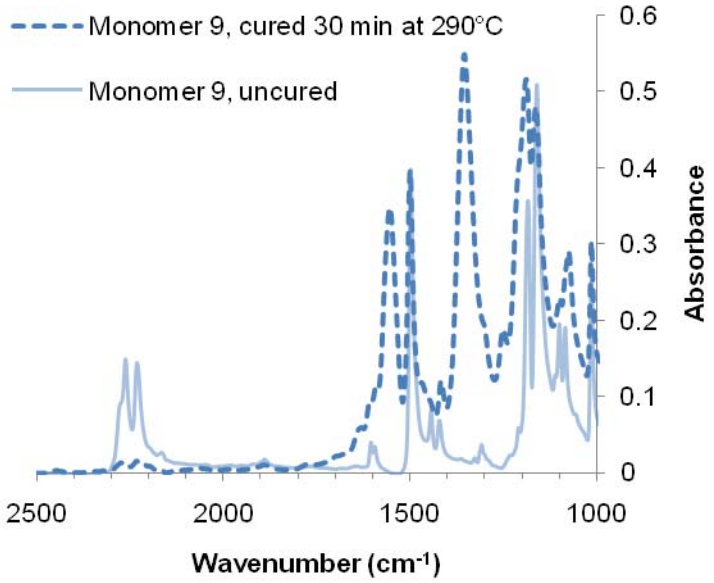

(b)

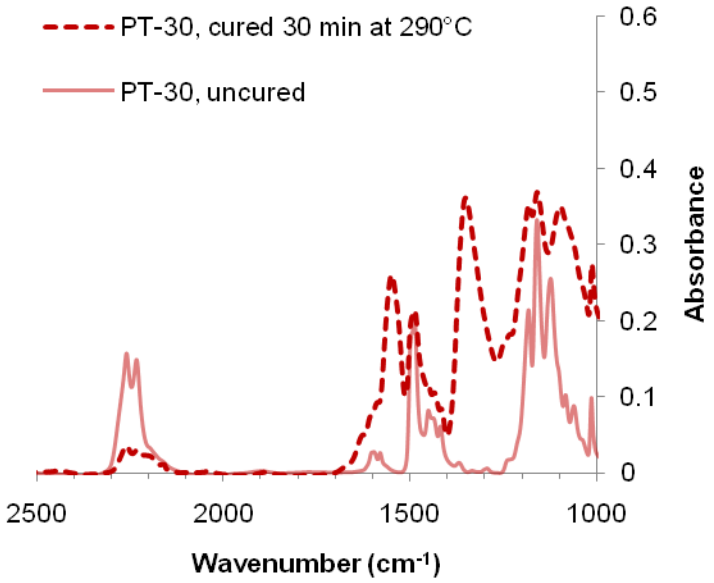

Figure 7: FT-IR spectrum of (a) monomer **9** and (b) PT-30 before and after single-step cure at 290 °C for 30 min.

(a)

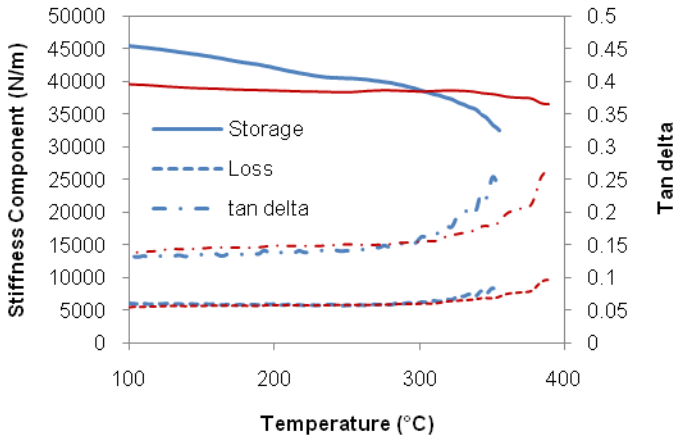

(b)

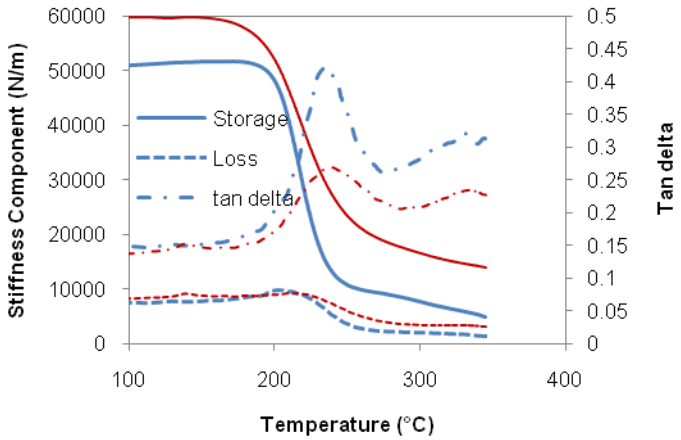

Figure 8: TMA of monomer **9** (thick blue lines) and PT-30 (thin red lines) after cure at 210 °C for 24 hr followed by 30 min. at 290 °C (a) before and (b) after 96 hr immersion in water at 85 °C. Note that (b) shows data collected during the cooling ramp due to bubble formation during heating.

(a)

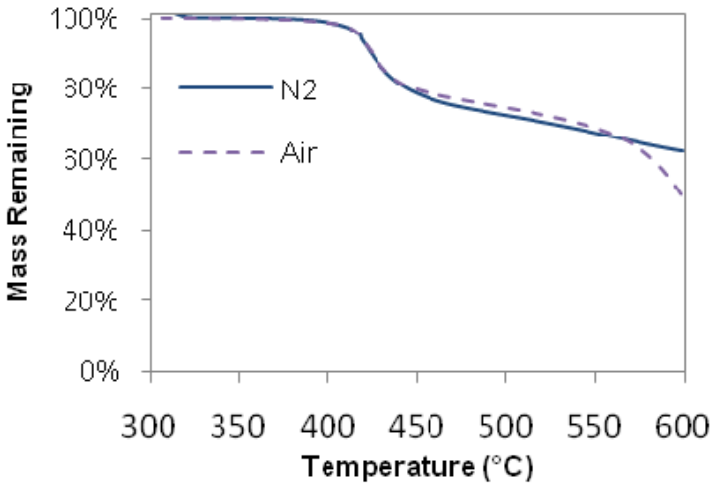

(b)

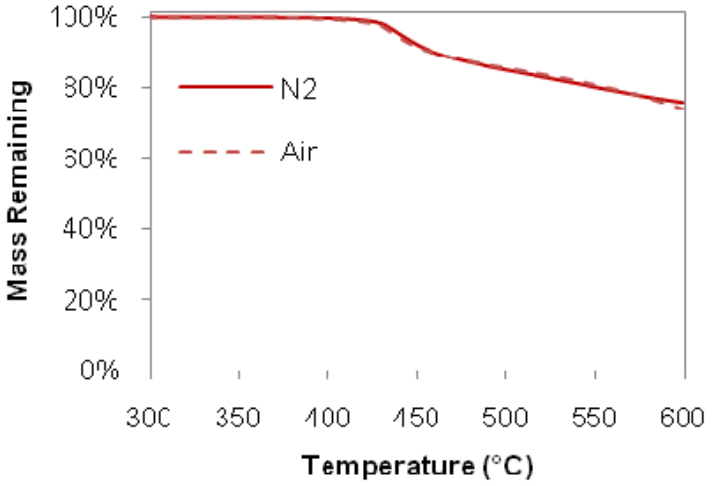

Figure 9: TGA of (a) monomer **9** and (b) PT-30 under nitrogen and air

Table 1

Physical data for monomer **9** and PT-30 cured 24 hours at 210 °C followed by 30 minutes of post-cure at 290 °C

Property	**cured** 9	**Primaset® PT-30**[a]
Density (g/cc)	1.251 ± 0.001	1.260 ± 0.001
Molar volume (cc/mol)	316.0 ± 0.4	302.7 ± 0.3
Cross-link density at full cure (N/cc)[b]	$3.811 \pm 0.004 \times 10^{21}$	$3.980 \pm 0.004 \times 10^{21}$

[a] Assumed structure as shown in Figure 1 with n=1

[b] Includes central branch point as a cross-link

Supplementary Content

"Synthesis, Cure Kinetics, and Physical Properties of a New Tricyanate Ester with Enhanced Molecular Flexibility"

Andrew J. Guenthner*[1], Matthew C. Davis[2], Kevin R. Lamison[3], Gregory R. Yandek[1], Lee R. Cambrea[2], Thomas J. Groshens[2], Lawrence C. Baldwin[2], and Joseph M. Mabry[1]

[1]Propulsion Directorate, Air Force Research Laboratory, Edwards AFB, CA 93524
[2]Naval Air Warfare Center, Weapons Division, China Lake, CA 93555
[3]ERC Corporation, Edwards AFB, CA 93524
**Correspondence to: andrew.guenthner@edwards.af.mil; 1-661-275-8020*

S1. Additional details of DSC measurements for kinetic analysis

Figures S-1a and S-1b illustrate typical DSC traces, baselines, temperature profiles, and regions used for analysis. Note that two baselines are required, an isothermal baseline during the cure process, and a non-isothermal baseline for the determination of residual enthalpy of cure. The isothermal baseline is significantly more reliable, being unaffected by changes in heat capacity during cure. Transient effects due to previous heating or cooling are present, but tend to disappear rapidly. On the other hand, for slow rates of cure, the results are more sensitive to the chosen isothermal baseline value, since the overall signal is small. In order to balance these issues, a fixed time interval of 30 minutes for isothermal cure was chosen (rather than waiting for complete cure to take place). This choice has the advantage that, as cure rates become slower, the residual enthalpy becomes correspondingly larger and thus contributes more towards the determination of the extent of cure achieved during the isothermal period, thereby limiting the accumulation of any errors in the measurement of conversion rate resulting from baseline errors. Conversely, for high rates of cure, any errors in the measurement of the small amount of residual cure have only a small influence on the much more precise (in relative terms) measurements of isothermal conversion rates.

In many cases, such as seen in Figure S-1a, a flat portion of the DSC response was available for baseline determination during both isothermal and non-isothermal cure. These flat portions generally showed only a decaying sinusoidal transient response at the start of the DSC program segment. The amplitudes and time constants for decay of these transient signals appeared to be nearly identical for all runs, enabling us to determine a point in time (5 minutes after the start of the non-isothermal heating, and from 2 to about 15 minutes after the start of the isothermal segment depending on the rate of cure) after which these transient effects were negligible. For the non-isothermal segments, in those cases where an obvious flat portion of the curve was not available (as in Figure S-1b), we simply chose a flat baseline coincident with the earliest point in time for which transient effects were negligible (5 minutes after the start of re-heating). For the isothermal segments, we included in the DSC program a five-minute "rest" at 120 °C (sufficient for disappearance of the transients), and in those cases where an obvious flat portion of the curve was not available (as in Figure S-1b), the signal value at the end of the isothermal rest period was used as a baseline value.

The observed differences between the "rest" value and the obvious baseline in the isothermal runs where both were available, and the observed differences between the earliest stable value and the obvious baseline in the available non-isothermal runs, were used to estimate the level of error in baseline determination that resulted from these procedures. Errors of 0.13 ± 0.05 mW for isothermal baselines, and 0.08 ± 0.04 mW for non-isothermal baselines, corresponding to average conversion rate errors of around 0.0001/s, were found. As explained previously, by limiting the time for isothermal cure, the overall errors in measured conversion due to both isothermal and non-isothermal baseline errors were limited to about 2% on average (based on a sensitivity analysis using the actual data). Because the residual cure took place over a limited temperature range, the baseline was not corrected for temperature dependence. Based on blank sample runs over similar temperature ranges, the error from using a flat rather than temperature-dependent baseline was estimated at around 0.04 mW for the

non-isothermal runs. A further sensitivity analysis of the effects of using altered baseline values on the values of the kinetic model parameters and subsequent effects on computed activation energies showed errors of up to 4 kJ/mol.

Another key issue when analyzing isothermal DSC data is the appropriate treatment of heat flows seen during temperature jumps. Since no temperature jump is truly instantaneous, there is a short period of rapid heating (1-2 minutes) followed by a rapid equilibration (about 1 minute). While the thermally activated cure rapidly accelerates as the temperature increases, the rate at which the temperature changes during equilibration rapidly decelerates. The result is that the rate of conversion (and hence, the DSC signal) tends to increase steadily with time after an apparent "turn on" during the rapid heating. Based on this observed phenomena, we found a "turn on" time of around 90 seconds after the programmed start of the temperature jump (at which point the sample is about 20 °C below the set point) described the data well. This observation held true even for experiments at 290 °C where the data during the temperature jump is quite noisy due to initiation of very rapid cure.

Based on the preceding discussion, the following parameters were adopted for analysis of the DSC data. Beginning at 90 seconds after the programmed jump, the DSC signal (corrected for heating rate based on a linear interpolation of data for isothermal and 5 °C / min heating at 120 °C) was utilized to compute the conversion via integration (and consideration of the residual exotherm as shown in Eq. 1). However, at conversions of less than 10%, none of the conversion or conversion rate data was used in subsequent analysis directly, only indirectly through tracking of accumulated conversion. (Since the isothermal cure of PT-30 at 210 °C did not reach 10% conversion in the allotted time, a kinetic analysis for use in determining the activation energy was not performed on the data). The reason for adopting a conversion-based limitation was the relative effect of the decaying sinusoidal transients discussed earlier. At slower conversion rates, these transients significantly affect the data for a longer period of

time, but since the conversion itself is slower, the extent of conversion affected by the transients turned out to be similar in all cases. The conversion-based limits were thus a simple way of handling these issues.

For samples cured at 290 °C, exceptionally rapid initial cure of the samples caused "spikes" in the data that lasted beyond 90 seconds after the start of the temperature jump. In these cases, the signals during the "spikes" were replaced by linearly interpolated values based on a zero conversion rate at 90 seconds after the start of the jump and the observed rates after the "spikes". The interpolated regions represented 1% of conversion for monomer **9** and 4% for PT-30, thus the interpolated data was never used directly in subsequent rate computations, only indirectly in the integrated calculation of conversions. Thus, for these two cases, the conversions (and therefore the absolute conversion rates) exhibit an additional uncertainty on the order of 1% for monomer **9** and 4% for PT-30. Based on a sensitivity analysis (via substitution of altered values in the regression analysis) to this larger error, however, the additional error in the activation energy was found to be just 0.2 kJ/mol for monomer **9** and 1.4 kJ/mol for PT-30.

S2. Additional details of data analysis

As explained in Section S1, only data from conversions greater than 10% was utilized for analysis. In addition, as explained in the Experimental section, data from conversions greater than 50% was not used due to the possible onset of diffusion-limited kinetics. At regular intervals of 15 seconds for cure at 270 °C and 290 °C, or 30 seconds otherwise, the DSC data were averaged over a span of 6 seconds, subtracted from the baseline determined as described in Section S1, and converted to a conversion rate based on Eq. 1. Cases exhibiting a clear maximum in the rate data were grouped by material type and averaged to create a constant parameter α_{max} for each material (0.49 ± 0.03 for monomer **9** and 0.53 ± 0.03 for PT-30). A consistent α_{max} was used due to the expectation that

individual “best fit” kinetic parameter values would be highly correlated, as is typical for the highly non-linear parametric modeling of the type undertaken. Fixing the value of α_{max} thus eliminated one source of unwanted variation.

The first step in the fitting process is illustrated in Figure S-2. Using limits of 10% and the first available data point at 15% conversion or greater, a linear regression of the conversion rate as a function of conversion was used to generate the intercept k_1' in Eq. 2. The linearity over this limited range was generally good, though only a limited number of data points were available. As pointed out in Section S1, the use of lower conversion values was not advisable due to the effect of transient signals on the raw DSC data.

Having determined k_1' and α_{max}, an initial guess for the value of m of 1 was chosen. From α_{max}, a corresponding trial value for n (here denoted n*) was simply calculated based on the approximation $\alpha_{max} = m / (m+n^*)$. Trial values of k_2' and m (here deonoted $k_2'^*$ and m*) were then determined by performing a linear regression on the left hand side of Eq. 3 as a function of ln α as illustrated in Figure S-3. Using the Newton-Raphson method, the root of the function m* - m, iteratively substituting m for m* (and k_2' for $k_2'^*$) at the end of each cycle, was located. The function m* - m was found to be well-behaved in the vicinity of this root. The use of different starting points did not result in the location of any additional roots. Moreover, the transformation provided by Eq. 3 resulted in effective linearization of the data only for values of m near 1. The values of $k_2'^*$, m*, and n* for which m* - m = 0 were then utilized as the best fit values for k_2', m, and n.

Once values of k_1', k_2', m, and n were computed for all cases (as listed in Table S-1), the m and n values (which are linearly related by definition) were averaged for each material. The mean values, $\overline{m}$ and $\overline{n}$ (also listed) were then used in subsequent calculations. Table S-2 lists the errors in k_1' and k_2' based on the standard errors of the intercepts of the relevant equations used in the regression, and of n

and m based on the standard error of the slope (linearly transformed for m). Note that the error in k_2' is multiplicative due to the logarithmic form of Eq. 2.

Figure S-4 illustrates the final step of the process, a linear regression using Eq. 4 to describe its left-hand side as a function of $\alpha^{\bar{m}}$ from which the intercept k_1 and slope k_2 were determined. As with the previous regressions, the data were well-described by a linear model. Table S-2 also lists the standard errors for k_1 and k_2 based only on the regression with fixed $\bar{m}$ and $\bar{n}$ values. Because of the numerous potential correlations between variables, no attempt to form a combined error estimate was made; the sensitivity analyses mentioned earlier, however, showed possible errors of as much as 0.0002/s in k_2 at lower temperatures, with errors of up to around 0.0001/s in k_1, which can be a substantial portion of the total value at lower temperatures, due mainly to uncertainty in the baselines.

For determination of the activation energy, a simple regression of k_2 as a function of temperature linearized according to the Arrhenius equation was used. No attempt to weight the values was undertaken due to the rough nature of the error estimates. The standard error of the slope parameter of the regression provides the basis for the ranges reported in Figure 6. To see the effect of otherwise difficult-to-quantify uncertainties (such as the choices made during modeling) on the activation energy, a few alternate Arrhenius analyses were performed. The alternate analyses included using the values of k_2' rather than k_2 to assess the effect of using mean values of the kinetic model exponents, excluding all data involving the alternate baselines (to assess the effect of possible baseline errors), and eliminating the kinetic model altogether. To accomplish the latter alternate analysis, it was noted that the conversion rate versus conversion data sets at different temperatures closely resembled linear transformations of one another except at very high and very low conversions. With the inclusion of small offset factors, a simple rescaling of the data at each temperature allowed for good

superposition of all curves, as demonstrated in Figures S-5a (monomer **9**) and S-5b (PT-30). The scale factors for each temperature were then treated as pseudo-rate constants in an Arrhenius analysis.

The results of the alternate analyses are shown in Table S-3; in all cases, monomer **9** has a lower activation energy than PT-30, and in fact, the difference is as large or larger for all alternative cases examined. We are thus confident that our choice of analytical methods did not lead to an incorrect conclusion about the relative activation energy of cure for the two monomers studied.

S3. Additional "wet" Tg data

As shown in Figure S-6, the first heating of samples of cured **9** and PT-30 subjected to immersion in boiling water for 96 hours produced large disturbances in the oscillatory TMA data. These disturbances were caused by the formation and subsequent collapse of bubbles throughout the sample once the glass transition temperature had been reached. It is possible to discern the initial stages of the glass transition in the data, prior to the signals becoming swamped with noise. The best estimate of the glass transition temperature in these cases is thus either the peak temperature for the loss component of the stiffness (if seen prior to onset of noise), or the onset temperature of significant noise in the loss component signal. Based on this criteria, glass transition temperatures around 235 °C and 225 °C were found for both cured **9** and cured PT-30, respectively, in agreement with the data from the subsequent cooling scan shown in Figure 8.

(a)

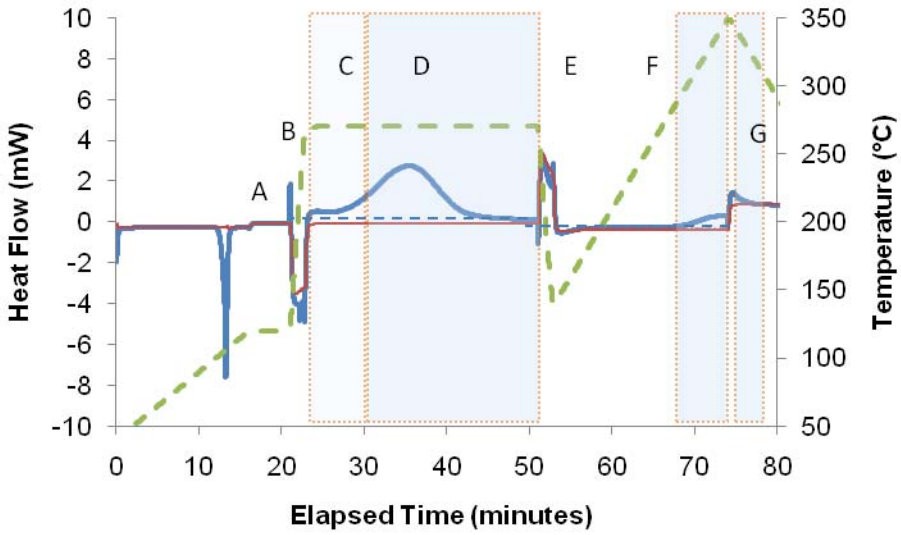

(b)

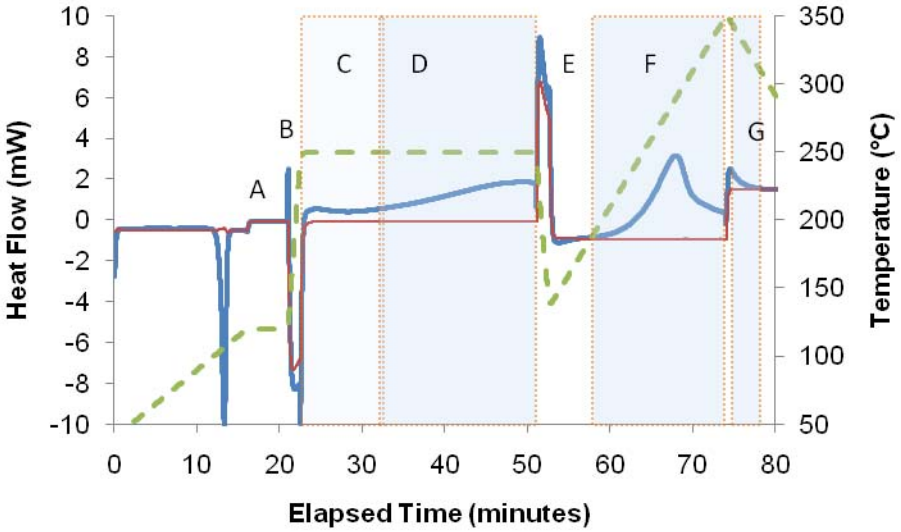

Figure S-1. Example plots of DSC signals as a function of scan time showing temperature (thick dashed line), unadjusted heat flow (solid thick line), well-defined baselines (thin dashed line), and alternate baselines (thin solid line) for monomer **9** cured at 270 °C (a) and 250 °C (b). The melting points are clearly visible, followed by (A) 5-minute isothermal rest to determine alternate baseline, (B) temperature jump (C) region in which conversion is tracked but no conversion or rate data are used directly for analysis, (D) isothermal analysis region, (E) temperature quench, (F) and (G) residual cure analysis regions

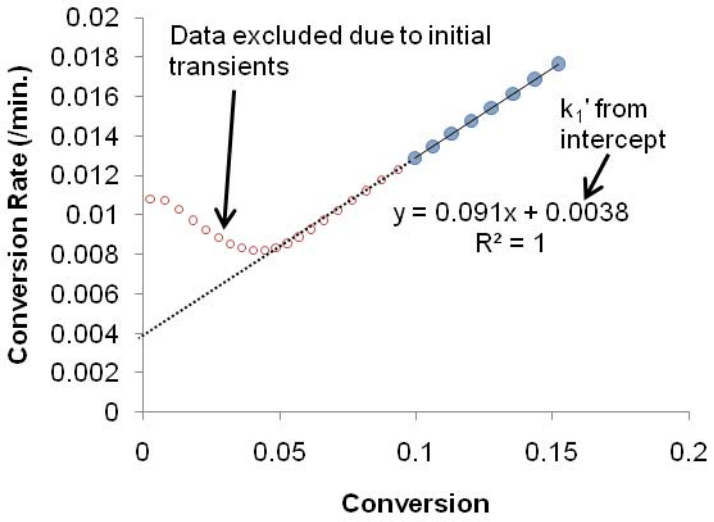

Figure S-2. Determination of k_1' via linear regression. The example is taken from the isothermal cure data for monomer **9** at 250 °C. The unfilled circles (as in Figure S-3 and S-4 also) show data affected by initial transients at conversions less than 0.1 that was not used in the regression.

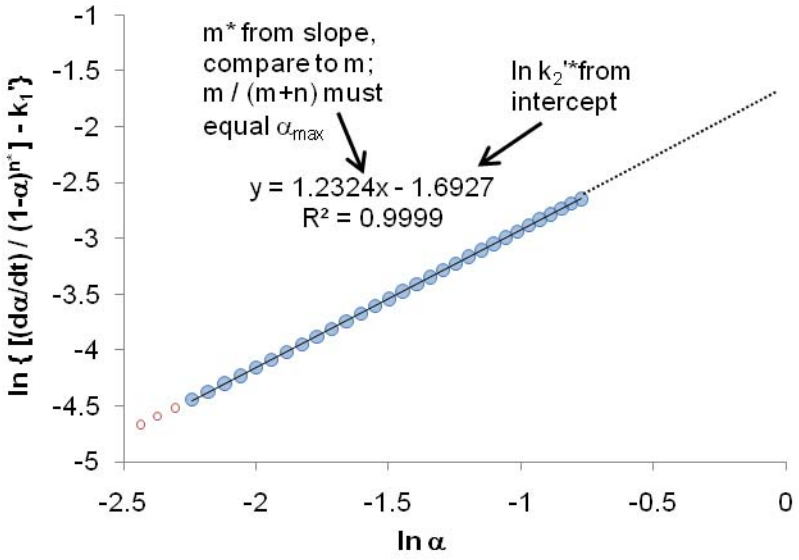

Figure S-3. Determination of k_2' and m via linear regression. The example is taken from the isothermal cure data for monomer **9** at 250 °C.

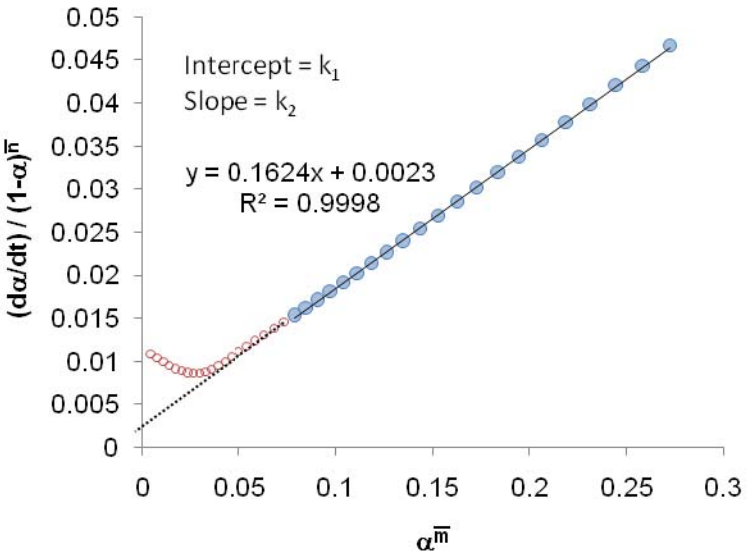

Figure S-4. Determination of k_1 and k_2 via linear regression. The example is taken from the isothermal cure data for monomer **9** at 250 °C.

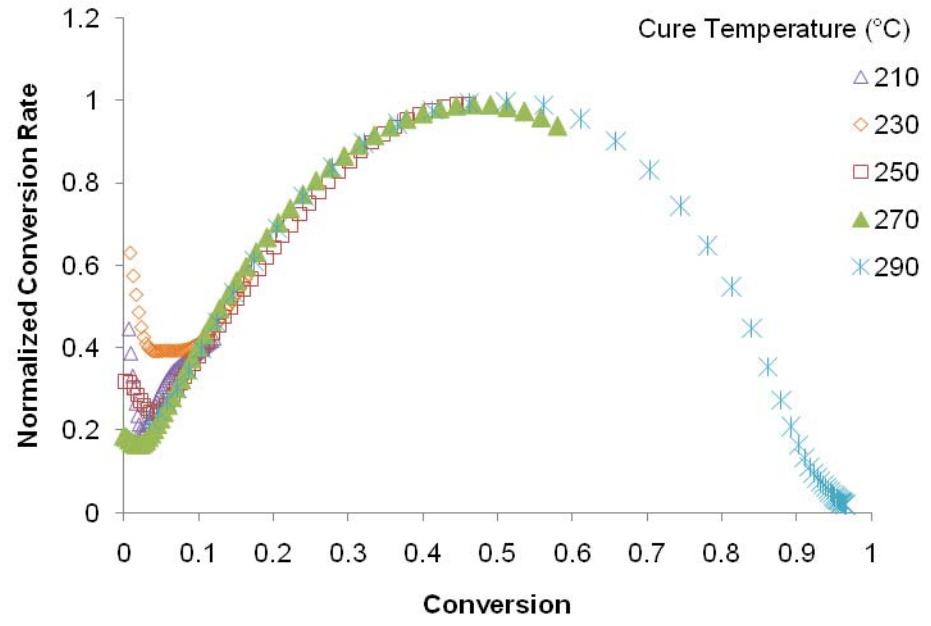

(b)

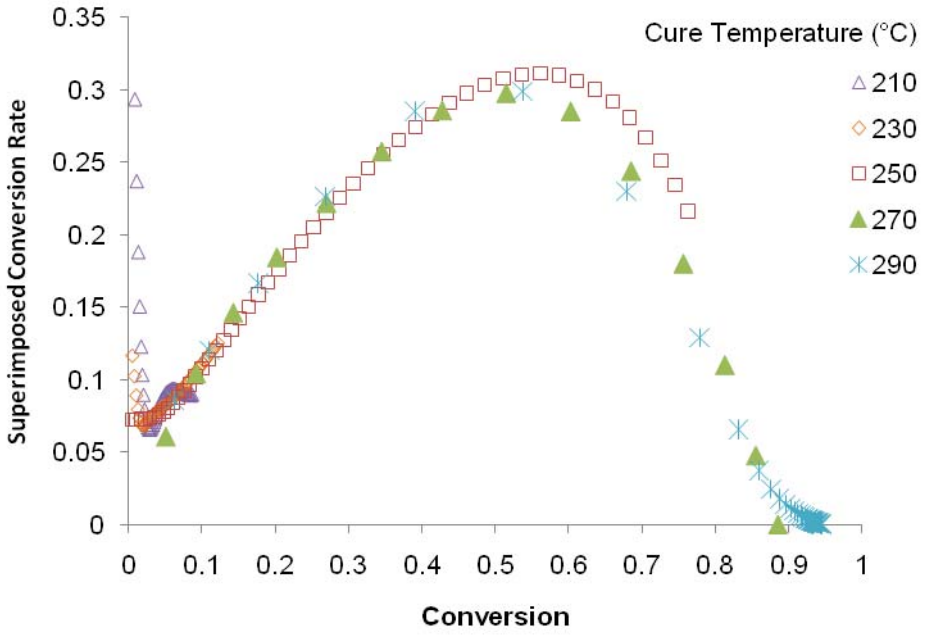

Figure S-5. Superimposed conversion rate curves for (a) monomer 9 and (b) PT-30; the superposition factors are for (a) Scaling: 0.006, 0.012, 0.034, 0.095, 0.2; Offset: -0.0026, 0.001, -0, 0.003, 0 (b) Scaling: 0.01, 0.05, 0.16, 0.42, 1; Offset: 0.0022, 0, 0, 0.005, 0, in ascending order of temperature, where the original rate (/min.) = displayed rate * scaling + offset.

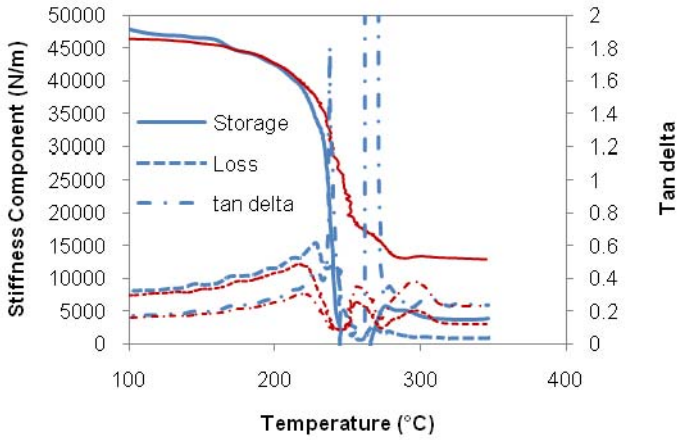

Figure S-6. Oscillatory TMA trace of cured **9** and cured PT-30 during heating after 96 hrs exposure to water at 85 °C. The thicker lines (blue) show data for cured **9**, the thinner lines (red) for PT-30.

Table S-1a

Kinetic model parameters for monomer **9** at various cure temperatures

°C	k_1' (/s)	k_2' (/s)	m	n	k_1 (/s)	k_2 (/s)	$\bar{m}$	$\bar{n}$
210	0.0000688	0.000332	1.128	1.174	0.0000690	0.000334	1.132	1.178
230	0.0000487	0.00109	1.247	1.298	0.0000398	0.000932	1.132	1.178
250	0.0000637	0.00307	1.232	1.283	0.0000358	0.00272	1.132	1.178
270	0.0000878	0.00663	1.052	1.095	0.000171	0.00718	1.132	1.178
290	0.000270	0.0156	1.111	1.157	0.000354	0.0157	1.132	1.178

Table S-1b

Kinetic model parameters for PT-30 at various cure temperatures

°C	k_1' (/s)	k_2' (/s)	m	n	k_1 (/s)	k_2 (/s)	$\bar{m}$	$\bar{n}$
230	0.0000405	0.000905	1.135	1.006	0.0000418	0.00105	1.235	1.095
250	0.000110	0.00391	1.286	1.140	0.0000676	0.00370	1.235	1.095
270	0.00103	0.00995	1.149	1.018	0.00111	0.0110	1.235	1.095
290	0.000744	0.0261	1.286	1.141	0.000543	0.0251	1.235	1.095

Table S-2a

Error estimates for kinetic model parameters for monomer **9** at various cure temperatures

°C	k_1' (/s)	k_2'[a] (/s)	m	n	k_1 (/s)	k_2 (/s)	$\bar{m}$	$\bar{n}$
210	0.0000048	1.053 x	0.023	0.024	0.0000005	0.000007	0.014	0.015
230	0.0000015	1.041 x	0.020	0.021	0.0000015	0.000015	0.014	0.015
250	0.0000002	1.003 x	0.002	0.002	0.0000011	0.000005	0.014	0.015
270	0.0000080	1.008 x	0.006	0.006	0.000008	0.00003	0.014	0.015
290	0.000012	1.014 x	0.009	0.010	0.000029	0.0001	0.014	0.015

[a] Since the computed parameter is ln k_2', the error estimate in k_2' itself is a multiplicative factor, e.g. one standard error in the value of k_2' at 210 °C is found by multiplying (or dividing) the estimate (found in the corresponding entry in Table S-1a) by 1.053. The errors for all other parameters represent ± 1 standard error of the regression.

Table S-2b

Error estimates for kinetic model parameters for PT-30 at various cure temperatures

°C	k_1' (/s)	k_2' (/s)	m	n	k_1 (/s)	k_2 (/s)	$\bar{m}$	$\bar{n}$
230	0.0000002	1.010 x	0.005	0.004	0.0000003	0.000004	0.009	0.008
250	0.0000005	1.014 x	0.010	0.008	0.0000078	0.00003	0.009	0.008
270	0.00003	1.017 x	0.011	0.010	0.00003	0.0001	0.009	0.008
290	0.000003	1.021 x	0.014	0.012	0.000062	0.0003	0.009	0.008

Table S-3

Results of alternative Arrhenius analyses of activation energy of monomer **9** and PT-30

Method	**E_a (kJ/mol)**	
	Monomer **9**	PT-30
As analyzed (Figure 6)	110	124
Use k_2' in place of k_2	108	130
Ignore data with alternate baselines	109	123
No kinetic model; graphically estimate scale factors needed to superimpose rate data	103	129